Carbon 234 (2025) 119951

Contents lists available at ScienceDirect

Carbon

journal homepage: www.elsevier.com/locate/carbon

Research paper

Ultraflat excitonic dispersion in single layer g-C_3N_4

Francesca Martini *, Pietro Nicolò Brangi, Pierluigi Cudazzo, Matteo Calandra

Department of Physics, University of Trento, Via Sommarive 14, 38123 Povo, Italy

ARTICLE INFO

Keywords:
Graphitic carbon nitride
Optical absorption
Excitonic dispersion
Two-dimensional materials
Water splitting
Self-trapped excitons

ABSTRACT

Single-layer graphitic carbon nitride (g-C_3N_4) is widely regarded as one of the most promising two-dimensional photocatalysts for hydrogen generation via water splitting. Despite its extensive study, limited information is available on its excitonic dispersion and velocity, critical parameters for achieving high charge mobility and efficient photogeneration. In this work, we employ many-body perturbation theory and the Bethe–Salpeter equation to provide a comprehensive description of the optical absorption and finite-momentum energy loss function for both s-triazine and tri-s-triazine structures. Our findings reveal the exciton dispersion and velocity, emphasizing the significant role of localized nitrogen lone pairs in producing remarkably flat excitonic bands with velocities that are two orders of magnitudes smaller than the typical one in two-dimensional materials and of the same order or smaller than the optical phonon frequencies in single layer g-C_3N_4. As the time-scale for inter-site exciton hopping is longer or similar to a phonon period, our results point to a highly non conventional exciton propagation.

1. Introduction

Polymeric g-C_3N_4 is a metal-free layered compound with a structure similar to that of graphite, high thermal and chemical stability, and non-toxicity. According to the literature [1–5], there exist two polytypes of g-C_3N_4, one composed of s-triazine units and the other of tri-s-triazine (often called heptazine) units. Even though tri-s-triazine g-C_3N_4 is considered to be the most stable one at ambient conditions [6], also s-triazine g-C_3N_4 has been experimentally obtained [7].

Polymericity, dimensionality, and the consequent reduced screening [8–10] are responsible for the strongly bound excitons with large binding energies of the order of 1–2 eV [1,3] occurring under photoexcitation in these materials. Excitons are electrically neutral, therefore their translational motions remain unaffected by electric fields. Indeed, excitons rather move through intramolecular or intermolecular diffusion. To be extracted as electric current or to initiate redox reactions, excitons must be dissociated within their lifetime and diffusion length, defined as the distance an exciton migrates before relaxing back to the ground state, into free charge carriers [11,12].

Both the exciton radiative lifetime [13] and diffusion [14] depend on the excitonic band structure. Previous calculations [3] of the radiative lifetimes neglected the excitonic dispersion (or assumed it to be parabolic for Wannier excitons). However, except for the simplest carbon nitride namely C_3N [15], neither calculations nor measurements of the exciton dispersions are available for these two polytypes in the literature. Furthermore, g-C_3N_4 is characterized by strongly localized lone pairs where the σ bond between a carbon and nitrogen atom is broken. Excitons coming from these lone pairs could also be highly localized, which could be detrimental to their use in electrocatalytic cells.

In this work, we calculate finite momentum energy loss function, the excitonic band dispersion and velocity for both polytypes in the framework of many-body perturbation theory (MBPT) [16,17] by using the GW approximation [18] and the Bethe–Salpeter equation (BSE) [17,19]. We show that the consequences of the localization of the lone pairs on the exciton dispersion are to generate ultraflat excitonic dispersions with negligible velocity. Finally, we point out that the time scales of exciton intersite hopping are similar or lower to a phonon period, suggesting a non-conventional incoherent propagation of the exciton strongly dressed by lattice deformations. This is a consequence of the localized nature of nitrogen lone-pairs and a unique feature of this compound.

The paper is structured as follows. In Section 2 we outline the methodology used in the paper. In Section 3 we describe in detail the results concerning crystal structure minimization, single particle electronic structure, exciton dispersion, and velocities. Finally, in Section 4 we address the relevance of our results for the understanding of exciton mobility in single-layer g-C_3N_4.

* Corresponding author.
E-mail addresses: francesca.martini-5@unitn.it (F. Martini), m.calandrabuonaura@unitn.it (M. Calandra).

https://doi.org/10.1016/j.carbon.2024.119951
Received 6 November 2024; Received in revised form 16 December 2024; Accepted 19 December 2024
Available online 26 December 2024

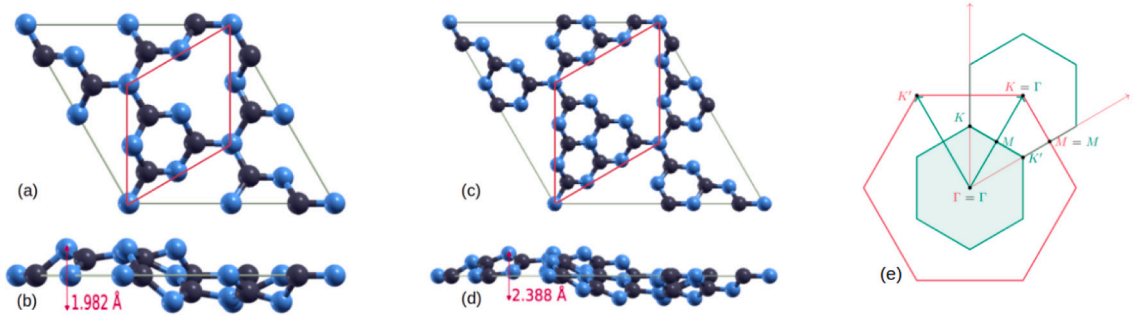

Fig. 1. (a) top and (b) side view of the crystal structure of s-triazine g-C_3N_4, (c) top and (d) side view of the crystal structure of tri-s-triazine g-C_3N_4(nitrogen atoms in blue, carbon atoms in black). In the top views ((a) and (c)) the 1 × 1 unit cell of the ideal structure is drawn in violet. (e) 1 × 1 (violet) and $\sqrt{3}\times\sqrt{3}R30°$ (green) first Brillouin zones and high symmetry points. (For interpretation of the references to color in this figure legend, the reader is referred to the web version of this article.)

2. Methods

The Density Functional Theory (DFT) [20,21] ground state calculations were performed using the QUANTUM ESPRESSO package [22,23]. We used optimized norm-conserving Vanderbilt pseudopotentials to compute the relaxed structure and the Kohn–Sham single-particle energies of the three systems. The KS-DFT exchange–correlation functional was approximated using GGA-PBE. For the structural optimization of the two systems, the accuracy on the structural minimization of the forces was set to 10^{-3} Ry/Bohr. For both polytypes, we used a Monkhorst–Pack k-point grid of 4 × 4 × 1, an energy cutoff of 100 Ry, and a charge density cutoff of 400 Ry in the charge density self-consistent calculation.

The many-body calculations were performed using the YAMBO code [24,25], adopting the Coulomb cutoff method [26] with a slab cutoff along the direction orthogonal to the lattice plane. Many-body corrections to the electronic band structure calculated using DFT are performed with the non-self-consistent perturbative GW (G_0W_0) approximation [27]. Bruneval–Gonze terminators [28] are applied to both the susceptibility and the self-energy calculations. Additionally, the plasmon-pole approximation is used [27]. In the case of s-triazine g-C_3N_4, we used a 14 × 14 × 1 k-point mesh, a 40 Ry cutoff on the plane waves, a 7 Ry cutoff on the response function, 300 bands for the susceptibility, and 200 for the self-energy. For tri-s-triazine g-C_3N_4 we used a 8 × 8 × 1 k-point mesh, a 50 Ry cutoff on the plane waves, a 6 Ry cutoff on the response function, and 400 bands for both the susceptibility and the self-energy.

The optical properties were then obtained by solving the BSE using the obtained quasi-particle (QP) corrections. Converged spectra are obtained on a 18 × 18 × 1 grid for s-triazine g-C_3N_4, and on a 14 × 14 × 1 grid for tri-s-triazine g-C_3N_4. Moreover, 8 valence and 8 conduction bands were included in the calculation for s-triazine g-C_3N_4, and 12 valence and 12 conduction bands for tri-s-triazine g-C_3N_4.

3. Results

3.1. Crystal and electronic structure

To understand the chemistry of g-C_3N_4 and why the corrugation of the structures emerges, it is useful to start by investigating how carbon and nitrogen atoms interact in the ideal flat structure. Nitrogen possesses an additional electron relative to carbon, so that when a nitrogen and a carbon atom are allowed to interact the additional electron is not used for bonding but acts as an electron donor and stays near nitrogen due to its higher electronegativity. Therefore, the two atoms form both σ and π bonds as if they were two carbon atoms. In fact, if one were to calculate the density of states of a graphene sheet with one of the two carbon atoms of the unit cell replaced by a nitrogen atom, he would see a similar behavior to that of graphene,

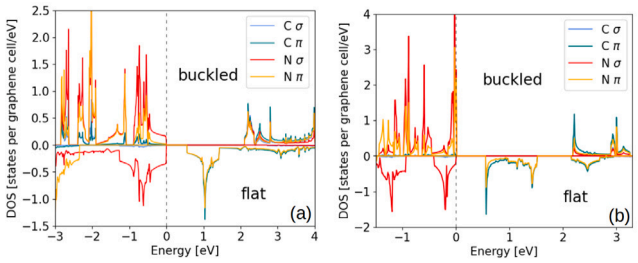

Fig. 2. Comparison between the projected density of states projected over the atomic orbitals of the buckled (top) and ideal flat (bottom) structures of (a) s-triazine and (b) tri-s-triazine g-C_3N_4.

with the appearance of the additional π bonding and antibonding states of nitrogen in the top valence and bottom conduction bands.

In Fig. 1(a) and (c) we show the non-corrugated ideal-structure of both g-C_3N_4 polytypes. The g-C_3N_4 matrix is characterized by wide openings due to the removal of some carbon atoms from the structure. This breaks the σ bond between carbon and nitrogen atoms. Therefore, there is an additional unpaired electron localized near nitrogen, which forms a lone pair with the preexisting electron. This lone pair exhibits strong localization and its energy is lifted with respect to the single electron occupation due to the Coulomb repulsion between the two charged particles. As a consequence, the top valence of the ideal flat structures is attributed to the lone pair and possesses N–σ character, while the bottom conduction band is primarily composed of π states originating from the two types of atoms, as shown in the bottom panels of Fig. 2(a) and 2 (b). Furthermore, the strong localization of lone pairs results in the emergence of flat bands in the electronic band structure, with the number of flat bands equal to the number of lone pairs present in the unit cell. These flat bands are evident as Van Hove singularities in the density of states in Figs. 2(a) and (b).

It is expected that the strong electrostatic repulsion between the lone pairs corrugates the structure so that the distance between opposite lone pairs in the triangular void is maximized, as it has been shown in previous works [2,3,29]. To verify this, we initially performed structural optimization with the atoms constrained in the plane. This resulted in highly imaginary phonon frequencies at zone center for modes involving out-of-plane displacements, indicating a dynamical instability in the planar structures. Following the approach of Ref. [3], we lifted the constraint, allowing the atoms to move out of plane, and conducted full structural optimization for the 1 × 1, 2 × 2, and $\sqrt{3}\times\sqrt{3}R30°$ supercells. We found that the most stable configuration adopts a $\sqrt{3}\times\sqrt{3}R30°$ supercell and is strongly corrugated (see Fig. 1(b) and (d)). The resulting structures exhibit real phonon frequencies, indicating the stability of the optimized configurations.

After structural optimization, the lattice constant is found to be 7.98 Å for s-triazine g-C_3N_4, and 11.8 Å for tri-s-triazine g-$C_3N_4$with the

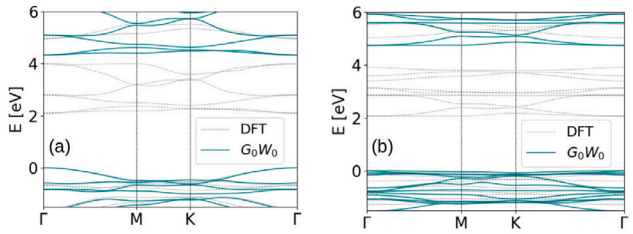

Fig. 3. Comparison between DFT and G_0W_0 electronic band structure of (a) s-triazine and (b) tri-s-triazine g-C_3N_4.

angle γ between the in-plane lattice vectors of 120° in agreement with previous literature [2,3]. The structures obtained have a layer thickness $d_z = 1.982$ Å for the s-triazine g-C_3N_4 and $d_z = 2.388$ Å for the tri-s-triazine case. Notice that the lattice constants of the $\sqrt{3} \times \sqrt{3}R30°$ unit cell for the flat and dynamically unstable structures are 8.27 Å and 12.33 Å for s-triazine and tri-s-triazine g-C_3N_4 respectively, meaning that corrugation shortens the in-plane distances between atoms.

By inspecting Fig. 2(a) and (b) it is clear that corrugation drastically changes the electronic and optical properties of both polytypes of g-C_3N_4. The corrugation not only opens the electronic gap but also, by distorting the planar structure, changes the symmetry of the bands, so that the top valence acquires also a π character of nitrogen. At the same time, the bottom conduction is now a hybridization of σ and π symmetry of both types of atoms involved.

In Fig. 3 the DFT electronic band structure with the G_0W_0 corrections is reported for both polytypes. As can be seen, both polytypes are direct gap semiconductors with the gap at the Γ point, in contrast to what Ref. [3] obtained; the discrepancy is probably due to a different level of corrugation of the structure. At the DFT level, the electronic gap is found to be 2.09 eV for s-triazine and 2.07 eV for tri-s-triazine g-C_3N_4. Furthermore, we can see the presence of the highly flat bands coming from the strong localization of the lone pairs, with effective masses m^* that range from $m^* = 1.78m_e$ for the most dispersive bands to $m^* > 30m_e$ for the flatter bands in tri-s-triazine g-C_3N_4 (with m_e we indicate the free electron mass).

However, while DFT is a widely used method for calculating ground-state properties, it can fail in the description of the electronic excited properties. To obtain more accurate and physically meaningful results, we go beyond DFT and employ the GW approximation for calculating the electronic band structure, and the BSE for the determination of neutral excitations and optical properties.

The many-body corrections open the DFT gap to 4.33 eV for s-triazine (Fig. 3(a)) and 4.75 eV for tri-s-triazine (Fig. 3(b)). Moreover, the GW corrections are not a rigid shift of the conduction band (scissor operator implemented in YAMBO), thus also changing the electronic dispersion with respect to the DFT one, especially for the valence band.

3.2. Optical absorption

The quasiparticle energies computed in the G_0W_0 approximation have then been employed in the optical absorption calculation of both polytypes via the state-of-the-art Bethe–Salpeter equation. Our results, for light with polarization parallel to the planar structure, are reported in Fig. 4(a) and (b) (solid green line). Both structures display a complex optical spectrum characterized by several features that spread up to more than 2 eV below the QP gap indicating the presence of strong excitonic effects. However, before analyzing in detail their nature, it is instructive to look at the optical spectra of the corresponding ideal flat structure [violet dotted line in Fig. 4(a) and (b)] in order to disentangle the effect of the corrugation on the optical properties of these systems.

Both spectra are characterized by a single dominant peak located at 4.5 eV for s-triazine and 4.0 eV for tri-s-triazine flat structures,

Table 1
Excitation energy and binding energy of the analyzed excitons for both polytypes.

		H_1	H_2	H_3	H_4	H_5
s-triazine g-C_3N_4	energy [eV]	2.79	3.06	3.32		
	binding energy [eV]	2.00	2.14	1.88		
tri-s-triazine g-C_3N_4	energy [eV]	2.61	2.99	3.55	4.07	4.09
	binding energy [eV]	2.57	2.42	1.95	1.13	1.30

together with a large multitude of lower energy dark excitons involving in-plane dipole forbidden $\sigma \rightarrow \pi$ transitions around the QP gap at Γ. The dominant peaks, on the other hand, originate from dipole optical active $\pi \rightarrow \pi$ transitions around the K (K') valley of the 1×1 Brillouin zone (BZ) [see violet line in Fig. 1(c)] that result in the formation of a resonant exciton in s-triazine and a bound exciton in tri-s-triazine. Interestingly, the energy and the character of these excitations are very similar to their intervalley counterpart at wave vector $\mathbf{q} = K$ involving $K \rightarrow K'$ transitions. This is a feature common to other materials with hexagonal lattice structures, such as boron nitrides (h-BN) [30,31] and transition metal dichalcogenides (TMDs) [32], and it is preserved in the buckled structure. As a matter of fact, in the $\sqrt{3} \times \sqrt{3}R30°$ supercell, both direct and intervalley excitons are folded at the Γ point of the $\sqrt{3}\times\sqrt{3}R30°$ BZ [see green region in Fig. 1(c)] and become both optical active in the presence of corrugation. This is the origin of the states H_4 and H_5 in the spectrum of tri-s-triazine which are responsible for the largest peak. It is blue-shifted of about 0.1 eV with respect to the corresponding feature in the flat structure as a consequence of the band gap opening induced by the corrugation. A similar behavior is found for the resonant exciton of s-triazine which is pushed above 5 eV (not shown).

Most importantly, the effect of the corrugation is to modify the hybridization of the highest occupied states that acquire a small amount of π component making optical active several excitons that were dark in the flat structures. From the analysis of the excitonic amplitudes, which define the weight of the different electron–hole pairs that build a given excitonic state, we can ascribe these excitations to transitions from the valence band dominated by the lone pair states to the first two conduction bands with π character.

In particular, in the case of s-triazine, the excitons H_1 and H_3 involve electron–hole pairs belonging to top-valence and bottom-conduction bands localized around the Γ and the K points, respectively. The exciton H_2, on the other hand, is associated to transitions between the top-valence band and the second conduction band around Γ. In the case of tri-s-triazine, the electron–hole pairs are mainly localized around the Γ point for the H_1 and H_4 excitons and around the M point for H_2. Moreover, while for s-triazine all these excitations are dominated by transitions between well defined pairs of bands, for tri-s-triazine they involve several bands in an energy window of 0.2 eV and 0.3 eV for the valence and conduction bands respectively. This multiband character of the tri-s-triazine excitons arising from a denser distribution of valence bands causes a significant enhancement of the excitonic effect as can be inferred from Table 1, where we compare the exciton and exciton binding energies [33] in the two polytypes.

Overall, in both systems the excitons display huge binding energies ranging between 2.57 eV and 1.30 eV which are larger than in other 2D semiconductors. This is related to the interplay of two cooperative effects: (*i*) the suppression of the long-range screening in 2D semiconductors that ensures a strong attractive electron–hole interaction [8]; (*ii*) the presence of weakly dispersive electronic bands that allows for coherent electron–hole pairs superpositions over a wide region of the BZ with negligible kinetic energy cost.

In the case of s-triazine g-C_3N_4, the first bright exciton H_1 is at 2.79 eV with a binding energy of 2.00 eV and leads to an optical gap in good agreement with the experimental values [34]. The optical gap of tri-s-triazine, set by the H_1 exciton at 2.61 eV with a binding energy of 2.57 eV, is also in line with the experimental value of 2.7 eV [35,36]

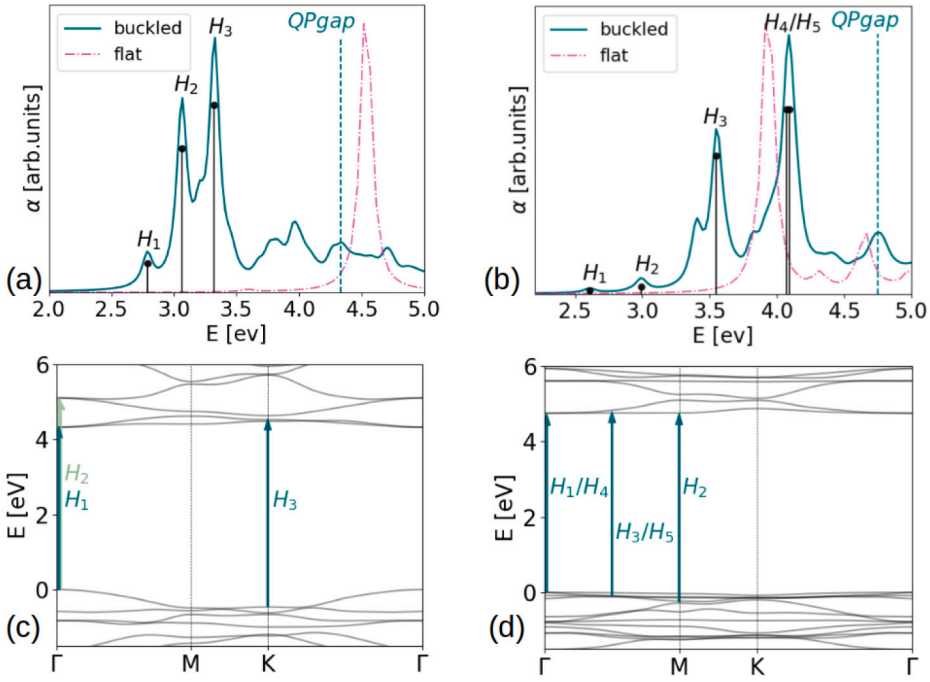

Fig. 4. (a) s-triazine and (b) tri-s-triazine optical absorption spectrum in the presence (green) and without (violet) corrugation. The vertical line represents the buckled structures' quasiparticle (QP) gap. Buckled (c) s-triazine and (d) tri-s-triazine relative transitions. The letters at the right of each arrow label the transition associated with each exciton. (For interpretation of the references to color in this figure legend, the reader is referred to the web version of this article.)

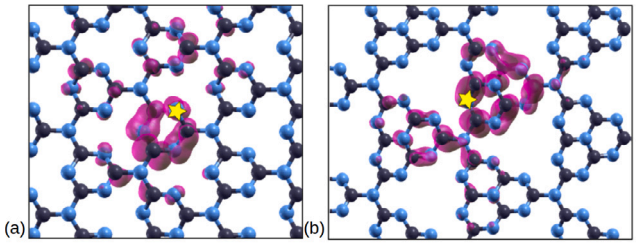

Fig. 5. Electronic charge distribution $|\Psi^{\lambda}(\mathbf{r_h}, \mathbf{r_e})|^2$ for a fixed position of the hole (slightly above a N atom and represented by a yellow star) for the exciton state H_1 for (a) s-triazine and (b) tri-s-triazine g-C_3N_4.

and previous calculations [29]. Unlike the case of the first polytype, the optical gap of tri-s-triazine g-C_3N_4 does not correspond to the lowest-energy solution of the BSE. Indeed, two degenerate dark excitons are present at lower energy (2.55 eV). The dark states are dipole-forbidden and therefore offer an alternative route for nonradiative decay of optical excitations, potentially impacting the luminescence yield [1].

The large binding energies of the H_1 excitons suggests that these states are spatially localized. This is confirmed by the plot in Fig. 5, where we report the electronic charge distributions of the H_1 excitons for both polytypes with the hole position fixed slightly above a N atom (yellow star). The excited electrons are delocalized on both the C and N atoms surrounding the hole and remain confined inside the unit cell, highlighting the Frenkel character of these excitations.

It is worth noting that, while for the tri-s-triazine the lowest excited state is the one with the highest binding energy, for s-triazine, the H_1 exciton is characterized by a binding energy smaller than the H_2 state. This behavior can be traced back to the dispersion of the conduction bands involved in the H_2 exciton that display a positive concavity similar to the valence bands. As a consequence, the valence and conduction bands are nearly parallel in a wide region of the BZ allowing for a strong mixing of independent electron–hole transitions at different wave vectors without increasing the exciton kinetic term.

3.3. Excitonic dispersion

The analysis carried out so far has shown how the low energy region of the optical spectrum of both polytypes is dominated by strong localized excitons associated with transitions between lone pairs and π states. The strong σ character of the lone pair states results in a small exciton dipole moment and thus in a long radiative lifetime that, as pointed out in Ref. [3], is of the order of hundreds of ns. This makes these systems particularly attractive for exciton control when properly engineered in heterojunctions in order to favor exciton dissociation. However, besides the long radiative lifetime, key properties for exciton control are the exciton mobility, which is linked to the exciton mass, and the exciton group velocity. All these quantities can be extracted from the exciton dispersion relation which can be directly probed in electron energy loss spectroscopy (EELS) and inelastic X ray scattering experiments.

From the structure of the excitonic Hamiltonian [19] the energy of a singlet exciton in a quantum state λ and wave vector $\mathbf{q}$ can be written as the sum of three contributions [37–42]: $E^s_{\lambda}(\mathbf{q}) = \mathcal{K}_{\lambda}(\mathbf{q}) + \mathcal{I}_{\lambda}(\mathbf{q}) + \mathcal{W}_{\lambda}(\mathbf{q})$. Here $\mathcal{W}$ and $\mathcal{I}$ arise from the direct and the exchange electron–hole interaction, respectively, while $\mathcal{K}$ is the kinetic term, which is directly related to the electronic band structure. Indeed it is given by the energy of the independent electron–hole pairs weighted by the excitonic amplitudes: $\mathcal{K}_{\lambda}(\mathbf{q}) = \sum_{vc\mathbf{k}}[\epsilon_c(\mathbf{k}+\mathbf{q}) - \epsilon_v(\mathbf{k})]|A^{vc\mathbf{k}}_{\lambda}(\mathbf{q})|^2$

In general, since the $\mathbf{q}$ dependence of $\mathcal{W}$ is related to the overlap integral between electronic wavefunctions localized on different units [37,38,40], its contribution to the exciton dispersion is always weaker than $\mathcal{K}$ and $\mathcal{I}$, which are related to the hopping scattering processes of the independent electron–hole pairs and the dipole–dipole interaction, respectively [38,40,42]. In particular, in standard 2D semiconductors the exchange electron–hole interaction at small $\mathbf{q}$ is characterized by a linear dispersion relation $\mathcal{I}_{\lambda}(\mathbf{q}) \approx 2\pi(\boldsymbol{\mu}_{\lambda} \cdot \hat{\mathbf{q}})^2|\mathbf{q}|$[37,43] set by the projection of the exciton dipole matrix element $\boldsymbol{\mu}_{\lambda}$ along the $\mathbf{q}$ direction. The kinetic term, on the other hand, reflects the electronic band dispersion and thus involves higher order contributions in $\mathbf{q}$. For example, in a two band system in the effective mass approximation

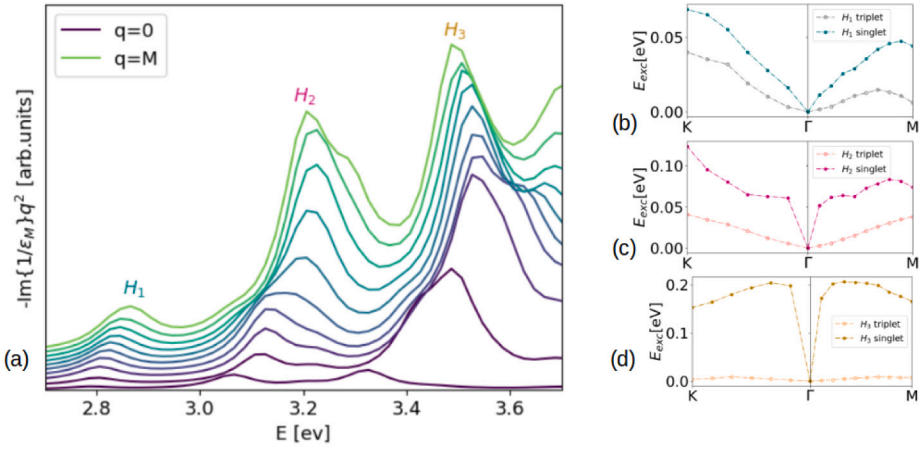

Fig. 6. s-triazine g-C_3N_4 (a) loss function for different values of transferred momentum along the direction $\Gamma - M$ starting from $\mathbf{q} \to 0$ (dark blue) to $\mathbf{q} = M$ (light green). Following the work of Ref. [37], the spectra are multiplied by q^2 for clarity. (b) H_1, (c) H_2, and (d) H_3 singlet (full dots) and triplet (empty dots) exciton dispersion in the direction $K - \Gamma - M$. In (b), (c), and (d) we plot $E^s(\mathbf{q}) - E^s(\mathbf{q} = 0)$ and $E^t(\mathbf{q}) - E^t(\mathbf{q} = 0)$. (For interpretation of the references to color in this figure legend, the reader is referred to the web version of this article.)

we have the simple relation $\mathcal{K}(\mathbf{q}) - \mathcal{K}(0) = \frac{|\mathbf{q}|^2}{2(m_h+m_e)}$, m_h and m_e being the hole and electron effective mass, respectively [42]. As a consequence, we can identify two regimes in the exciton dispersion: (*i*) small wave vectors, where the dispersion is linear and is governed by the exchange electron–hole interaction; (*ii*) large wave vectors, where the dispersion is not linear and it is mainly governed by the kinetic term and eventually $\mathcal{W}$. The crossover between the two regimes is set by the strength of the exciton dipole and the dispersion of the electronic bands. In particular, the more the exciton is localized as a consequence of the presence of weakly dispersive electronic bands (this is what one expects for a 2D Frenkel-like excitons) the larger the linear region in the BZ. For triplet excitons the dispersion is given by the relation $E^t_\lambda(\mathbf{q}) = \mathcal{K}_\lambda(\mathbf{q}) + \mathcal{W}_\lambda(\mathbf{q})$ due to the lack of the exchange electron–hole interaction and thus it is dominated by the kinetic term.

In Fig. 6(a) we report the electron energy loss function of s-triazine evaluated at different $\mathbf{q}$ along the ΓM direction. The three features display a positive dispersion for $\mathbf{q} \to 0$. However, while for the first peak associated with the H_1 exciton, the positive dispersion extends up to the boundary of the BZ, for the higher energy peaks associated with the H_2 and H_3 excitons the dispersion flattens at larger $\mathbf{q}$ and then inverts its slope. To gain further insight into the behavior of the loss function, we compare in Fig. 6(b), (c), and (d) the dispersion of the excitons H_1, H_2, and H_3 with the dispersion of corresponding states in the triplet channel that, at the Γ point, are located at 2.55 eV, 2.64 eV, and 3.10 eV respectively. Moreover, for each curve, the origin of the energy axis has been fixed at 0 at the Γ point. As expected, all the singlet states display a linear dispersion for $\mathbf{q} \to 0$ with a slope that progressively increases from the exciton H_1 to the exciton H_3 consistently with the behavior of exciton dipole moment that sets the exciton oscillator strength in the spectra. Then, for larger $\mathbf{q}$, they follow approximately the behavior of the corresponding triplet states that is dominated by the kinetic term. It is important to note that, despite the strong spatial localization of these states, the linear regime of the exciton dispersion is restricted to a small region around Γ. This is a consequence of the small exciton dipole moments associated with the transitions between the lone pairs and the π states.

In Fig. 7(a) we show the loss function of tri-s-triazine. The dominant peak associated with the H_5 exciton involving $\pi \to \pi$ transitions displays a strong positive dispersion characterized by a bandwidth of 0.42 eV. The comparison with the behavior of the corresponding triplet state located 0.2 eV below the H_5 peak [see Fig. 7(c)] clearly shows how the dispersion of this excitation is completely determined by the exchange electron–hole interaction, as expected for localized Frenkel excitons. In particular, the exciton group velocity at Γ is 0.38 nm/fs, which is more than two times larger than in other 2D semiconductors such as MoS_2 [14], hosting more delocalized Wannier-like excitons. This is a direct consequence of the large exciton dipole moment related to the spatial localization, which ensures a strong overlap between electron and hole states, as well as to the dominant π character of both valence and conduction states that enhances the oscillator strength of the independent electron–hole pairs that build the exciton. In addition, due to the weak dispersion of the electronic bands, the kinetic term does not remarkably affect the linear dispersion of the singlet exciton, which is preserved over a wide region of the BZ. The situation is quite different for the other features at 3.50 eV that, being related to the lone pairs, are characterized by a small exciton dipole moment and display a weak positive dispersion in analogy with the other polytype.

More complex is the behavior of the low energy region of the spectrum between 2.50 eV and 3.25 eV [see inset in Fig. 7(a)]. Here, higher order terms in the multipole expansion of the oscillator strength activate dipole forbidden transitions as $\mathbf{q}$ increases, leading to the appearance of two additional features at 2.71 eV, above the H_1 exciton and 2.90 eV, below the H_2 exciton, respectively. Having zero exciton dipole moment, their behavior as a function of $\mathbf{q}$ is mainly set by the $\mathcal{K}$ and $\mathcal{W}$ terms and results almost non-dispersive.

Interestingly, despite the presence of the exchange electron–hole interaction, the H_1 exciton, which defines the onset of the spectrum, displays a weak negative dispersion, linear for $\mathbf{q} \to 0$. As can be understood from Fig. 7(b), this behavior is induced by the kinetic term that, contrary to what one might expect in the effective mass approximation, does not reflect the dispersion of the electronic band structure but is characterized by a linear dispersion with negative slope. Due to the small exciton dipole moment, the exchange electron–hole interaction only attenuates the effect of the kinetic term without changing the slope of the energy curve. The unusual behavior of $\mathcal{K}(\mathbf{q})$ arises from the fact that, as $\mathbf{q}$ increases, the strength of the excitonic amplitude is progressively transferred to lower energy electron–hole pairs. Thus, it is a pure excitonic effect related to the multiband nature of the tri-s-triazine excitons that cannot be explained in terms of the electronic band structure alone.

It is important to note that this effect is essentially absent in the triplet channel [green lines in Fig. 7(b)] where the kinetic term follows the typical parabolic dispersion dictated by the electronic bands. This indicates that the different behavior of the excitonic amplitude for the singlet exciton must be ascribed to the exchange electron–hole interaction which is the only contribution absent in the triplet channel. As a matter of fact, in the optical limit, the exchange electron–hole contribution to the excitonic Hamiltonian is proportional to the dipole

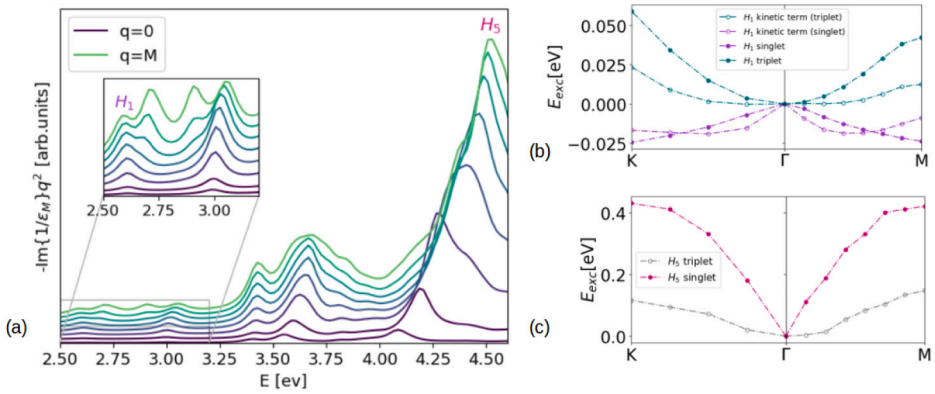

Fig. 7. tri-s-triazine g-C_3N_4 (a) loss function for different values of transferred momentum along the direction $\Gamma - M$ starting from $\mathbf{q} \to 0$ (dark blue) to $\mathbf{q} = M$ (light green). Following the work of Ref. [37], the spectra are multiplied by q^2 for clarity. (b) H_1 singlet (full purple dots) and triplet (full green dots) exciton dispersion, together with the kinetic terms calculated using the singlet (empty purple dots) and triplet (empty green dots) excitonic amplitudes, and (c) H_5 singlet (full dots) and triplet (empty dots) exciton dispersion in the direction $K - \Gamma - M$. In (b) and (c) we plot $E^s(\mathbf{q}) - E^s(\mathbf{q} = 0)$ and $E^t(\mathbf{q}) - E^t(\mathbf{q} = 0)$ and the same for the kinetic terms. (For interpretation of the references to color in this figure legend, the reader is referred to the web version of this article.)

matrix elements between occupied and empty states. In the present case, due to the dominant π character of the conduction bands, only hole states with non-negligible π character are involved in exchange electron–hole scattering processes. From Fig. 2(b) we can see that these states are localized in energy close to the top of the valence band so that the final effect of the exchange electron–hole interaction in the formation of the excitonic state is to foster the mixing of electron–hole pairs with lower energy close to the QP gap. At $\mathbf{q} = 0$ the long-range part of the exchange electron–hole interaction is zero but it increases linearly with $|\mathbf{q}|$ resulting in a progressive transfer of the strength of the excitonic amplitude to lower energy electron–hole pairs.

3.4. Exciton velocities and unconventional exciton propagation

Starting from the exciton dispersion we can evaluate the exciton group velocities for the lowest excited states below 3.3 eV which are directly coupled with the visible light. We find that in this region of the absorption spectrum the exciton group velocities are two orders of magnitude smaller than in other 2D semiconductors such as TMDs and phosphorene [14] ranging between 0.01 nm/fs and 0.04 nm/fs for both polytypes. This leads to a small exciton mobility and diffusion coefficient that could be detrimental for practical applications in electrocatalytic cells. From the analysis of the dispersion of these excitons associated with transitions between lone pairs and empty π states, we can ascribe the extremely small exciton group velocity to two basic peculiarities of these materials: the strong localization of the lone pairs that give rise to weakly dispersive electronic bands and their strong σ character that results in a small exciton dipole moment, being $\sigma \to \pi$ transitions dipole forbidden.

Nevertheless, it is important to note that, due to the weak exciton dispersion, exciton diffusion in these materials could be more complex than what one expects in the simple coherent exciton wave packet picture [14] where the diffusion coefficient is set by the exciton–phonon scattering rate and the exciton group velocity [44]. Indeed, the exciton bandwidth for the H_1 exciton that sets the optical gap in both systems is 40 meV in s-triazine and 20 meV in tri-s-triazine. In both cases it is of the same order or smaller than the typical optical phonon frequencies of these materials ranging between 12 meV and 62 meV. This means that the time scale for the inter site hopping scattering processes of the exciton is longer than the characteristic period of a lattice vibration. Under these conditions the coupling to lattice vibrations could induce exciton self-trapping [45,46] so that the exciton does not propagate like a wave packet with a well defined group velocity but rather like an incoherent local excited state dressed by a lattice deformation that hops from one crystal unit to another [44].

4. Conclusions

In this work, we provide a comprehensive description of the optical absorption and finite-momentum energy loss function for both s-triazine and tri-s-triazine structures. Our findings highlight the role of localized nitrogen lone pairs in producing remarkably flat excitonic bands with velocities that are two orders of magnitudes smaller than the typical one in 2D materials. The flatness of the exciton dispersion is accompanied by several peculiar behaviors, such as negative dispersing excitons in tri-s-triazine. Our results point to a non-conventional exciton propagation strongly dressed by lattice deformations, a unique feature of g-C_3N_4.

CRediT authorship contribution statement

Francesca Martini: Writing – review & editing, Writing – original draft, Visualization, Validation, Methodology, Investigation, Formal analysis, Data curation. **Pietro Nicolò Brangi:** Writing – review & editing, Methodology, Investigation, Formal analysis, Data curation. **Pierluigi Cudazzo:** Writing – review & editing, Writing – original draft, Validation, Supervision, Methodology, Investigation, Formal analysis, Conceptualization. **Matteo Calandra:** Writing – review & editing, Writing – original draft, Validation, Supervision, Resources, Project administration, Methodology, Investigation, Funding acquisition, Formal analysis, Conceptualization.

Declaration of competing interest

The authors declare the following financial interests/personal relationships which may be considered as potential competing interests: Matteo Calandra reports financial support was provided by Autonomous Province of Trento. If there are other authors, they declare that they have no known competing financial interests or personal relationships that could have appeared to influence the work reported in this paper.

Acknowledgments

We acknowledge fruitful discussions with Michele Orlandi and Antonio Miotello. We acknowledge support from the project Produrre Idrogeno in Trentino - H2@TN (PAT-Trento). Funded by the European Union, Next Generation EU, mission 4, component 2, CUP E63C22000970007. We acknowledge EUROHPC (EHPC-REG-2024R01-06), for the availability of high performance computing resources and support.

References

[1] W. Wei, T. Jacob, Phys. Rev. B—Condens. Matter Mater. Phys. 87 (8) (2013) 085202.
[2] X. Shi, J. Li, T. Ouyang, C. Zhang, C. Tang, C. He, J. Zhong, et al., Physica E: Low-Dimensional Syst. Nanostruct. 128 (2021) 114535.
[3] M. Re Fiorentin, F. Risplendi, M. Palummo, G. Cicero, ACS Appl. Nano Mater. 4 (2) (2021) 1985–1993.
[4] S.N. Steinmann, S.T. Melissen, T. Le Bahers, P. Sautet, J. Mater. Chem. A 5 (10) (2017) 5115–5122.
[5] J. Gracia, P. Kroll, J. Mater. Chem. 19 (19) (2009) 3013–3019.
[6] E. Kroke, M. Schwarz, E. Horath-Bordon, P. Kroll, B. Noll, A.D. Norman, New J. Chem. 26 (5) (2002) 508–512.
[7] G. Algara-Siller, N. Severin, S.Y. Chong, T. Björkman, R.G. Palgrave, A. Laybourn, M. Antonietti, Y.Z. Khimyak, A.V. Krasheninnikov, J.P. Rabe, et al., Angew. Chem, Int. Ed. 53 (29) (2014) 7450–7455.
[8] P. Cudazzo, I.V. Tokatly, A. Rubio, Phys. Rev. B—Condens. Matter Mater. Phys. 84 (8) (2011) 085406.
[9] L.V. Keldysh, JEPT Lett. 29 (1979) 716.
[10] P. Cudazzo, C. Attaccalite, I.V. Tokatly, A. Rubio, Phys. Rev. Lett. 104 (2010) 226804.
[11] M. Rahman, H. Tian, T. Edvinsson, Angew. Chem. 132 (38) (2020) 16418–16433.
[12] D.E. Markov, E. Amsterdam, P.W. Blom, A.B. Sieval, J.C. Hummelen, J. Phys. Chem. A 109 (24) (2005) 5266–5274.
[13] H.-Y. Chen, V.A. Jhalani, M. Palummo, M. Bernardi, Phys. Rev. B 100 (7) (2019) 075135.
[14] D.Y. Qiu, G. Cohen, D. Novichkova, S. Refaely-Abramson, Nano Lett. 21 (18) (2021) 7644–7650.
[15] M. Bonacci, M. Zanfrognini, E. Molinari, A. Ruini, M.J. Caldas, A. Ferretti, D. Varsano, Phys. Rev. Mater. 6 (3) (2022) 034009.
[16] G. Strinati, La Rivista Nuovo Cimento (1978-1999) 11 (12) (1988) 1–86.
[17] G. Onida, L. Reining, A. Rubio, Rev. Modern Phys. 74 (2) (2002) 601.
[18] L. Hedin, Phys. Rev. 139 (3A) (1965) A796.
[19] M. Rohlfing, S.G. Louie, Phys. Rev. B 62 (8) (2000) 4927.
[20] P. Hohenberg, W. Kohn, Phys. Rev. 136 (3B) (1964) B864.
[21] W. Kohn, L.J. Sham, Phys. Rev. 140 (4A) (1965) A1133.
[22] P. Giannozzi, S. Baroni, N. Bonini, M. Calandra, R. Car, C. Cavazzoni, D. Ceresoli, G.L. Chiarotti, M. Cococcioni, I. Dabo, et al., J. Phys.: Condens. Matter 21 (39) (2009) 395502.
[23] P. Giannozzi, O. Andreussi, T. Brumme, O. Bunau, M.B. Nardelli, M. Calandra, R. Car, C. Cavazzoni, D. Ceresoli, M. Cococcioni, et al., J. Phys.: Condens. Matter 29 (46) (2017) 465901.
[24] A. Marini, C. Hogan, M. Grüning, D. Varsano, Comput. Phys. Comm. 180 (8) (2009) 1392–1403.
[25] D. Sangalli, A. Ferretti, H. Miranda, C. Attaccalite, I. Marri, E. Cannuccia, P. Melo, M. Marsili, F. Paleari, A. Marrazzo, et al., J. Phys.: Condens. Matter. 31 (32) (2019) 325902.
[26] C.A. Rozzi, D. Varsano, A. Marini, E.K.U. Gross, A. Rubio, Phys. Rev. B 73 (2006) 205119.
[27] M.S. Hybertsen, S.G. Louie, Phys. Rev. B 34 (8) (1986) 5390.
[28] F. Bruneval, X. Gonze, Phys. Rev. B—Condens. Matter Mater. Phys. 78 (8) (2008) 085125.
[29] J. Sun, X. Li, J. Yang, Nanoscale 10 (8) (2018) 3738–3743.
[30] T. Galvani, F. Paleari, H.P. Miranda, A. Molina-Sánchez, L. Wirtz, S. Latil, H. Amara, F. Ducastelle, Phys. Rev. B 94 (12) (2016) 125303.
[31] G. Marini, M. Calandra, P. Cudazzo, Nano Lett. 24 (20) (2024) 6017–6022.
[32] X. Xu, W. Yao, D. Xiao, T.F. Heinz, Nat. Phys. 10 (5) (2014) 343–350.
[33] Because of the multiband character of excitons in g-C_3N_4, here we define the exciton binding energy as: $EBE^{\lambda} = \sum_{vc\mathbf{k}}[\epsilon_c(\mathbf{k}+\mathbf{q}=\mathbf{0}) - \epsilon_v(\mathbf{k})]|A_{\lambda}^{vc\mathbf{k}}(\mathbf{q}=0)|^2$ where $A_{\lambda}^{vc\mathbf{k}}(\mathbf{q}=\mathbf{0})$ is the excitonic amplitude at $\mathbf{q}$=0 for the state λ.
[34] P. Praus, Carbon Lett. 32 (3) (2022) 703–712.
[35] A. Kumar, P. Kumar, C. Joshi, M. Manchanda, R. Boukherroub, S.L. Jain, Nanomaterials 6 (4) (2016) 59.
[36] K. Maeda, X. Wang, Y. Nishihara, D. Lu, M. Antonietti, K. Domen, J. Phys. Chem. C 113 (12) (2009) 4940–4947.
[37] P. Cudazzo, L. Sponza, C. Giorgetti, L. Reining, F. Sottile, M. Gatti, Phys. Rev. Lett. 116 (6) (2016) 066803.
[38] P. Cudazzo, M. Gatti, A. Rubio, F. Sottile, Phys. Rev. B 88 (2013) 195152.
[39] M. Gatti, F. Sottile, Phys. Rev. B 88 (2013) 155113.
[40] P. Cudazzo, F. Sottile, A. Rubio, M. Gatti, J. Phys.: Condens. Matter. 27 (11) (2015) 113204.
[41] J. Koskelo, G. Fugallo, M. Hakala, M. Gatti, F. Sottile, P. Cudazzo, Phys. Rev. B 95 (2017) 035125.
[42] R.S. Knox, Solid State Phys. 3 (1963).
[43] D.Y. Qiu, T. Cao, S.G. Louie, Phys. Rev. Lett. 115 (17) (2015) 176801.
[44] G.F. Bassani, V.M. Agranovich, Electronic Excitations in Organic Based Nanostructures, Elsevier, 2003.
[45] S. Ismail-Beigi, S.G. Louie, Phys. Rev. Lett. 95 (2005) 156401.
[46] Z. Dai, C. Lian, J. Lafuente-Bartolome, F. Giustino, Phys. Rev. Lett. 132 (2024) 036902.